Cell wound repair in *Drosophila* occurs through three distinct phases of membrane and cytoskeletal remodeling

Maria Teresa Abreu-Blanco, Jeffrey M. Verboon, and Susan M. Parkhurst

Division of Basic Sciences, Fred Hutchinson Cancer Research Center, Seattle, WA 98109

When single cells or tissues are injured, the wound must be repaired quickly in order to prevent cell death, loss of tissue integrity, and invasion by microorganisms. We describe *Drosophila* as a genetically tractable model to dissect the mechanisms of single-cell wound repair. By analyzing the expression and the effects of perturbations of actin, myosin, microtubules, E-cadherin, and the plasma membrane, we define three distinct phases in the repair process—expansion, contraction, and closure—and identify specific components required during each phase. Specifically, plasma membrane mobilization and assembly of a contractile actomyosin ring are required for this process. In addition, E-cadherin accumulates at the wound edge, and wound expansion is excessive in E-cadherin mutants, suggesting a role for E-cadherin in anchoring the actomyosin ring to the plasma membrane. Our results show that single-cell wound repair requires specific spatial and temporal cytoskeleton responses with distinct components and mechanisms required at different stages of the process.

Introduction

Most cells of the body are subjected to physiological events during normal functions that can lead to disruption of the cell's plasma membrane (McNeil and Steinhardt, 2003; Martin and Parkhurst, 2004). The capacity of single cells to repair day-to-day wear-and-tear injuries, as well as traumatic ones, is fundamental for maintaining tissue integrity. In addition, cells can become damaged as a result of disease, such as the fragile skin cells of Epidermolysa bullosa simplex patients and myocytes of Duchenne muscular dystrophy patients, or in response to bacterial toxin lesions (Coulombe et al., 1991; Petrof et al., 1993; Gilbert, 2002). Upon disruption of the plasma membrane, an influx of calcium signals the deployment of vesicles that fuse with each other and with the plasma membrane to plug the hole (McNeil and Kirchhausen, 2005). After the membrane has been sealed, repair of the cell's cortical cytoskeleton is required to reestablish a normal cytoarchitecture (Fein and Terasaki, 2005). Cytoskeleton remodeling is mediated by a contractile ring of F-actin and myosin, accompanied by a radial arrangement of microtubules, and requires a specific signal transduction response involving Rho family GTPases (Bement et al., 2007).

Drosophila has recently emerged as a genetic model for studying multicellular wound repair (Kiehart et al., 2000; Wood et al., 2002; Galko and Krasnow, 2004; Stramer et al., 2005). Here we show that the *Drosophila* embryo is an excellent model in which to interrogate the single-cell wound-healing process. We use 4D in vivo microscopy along with pharmacological and genetic manipulations to define the series of changes that occur during three distinctive phases in response to wounding. We find that specific molecular components including actin, myosin, microtubules, and the plasma membrane respond dynamically during cell wound repair, and demonstrate that perturbations of each of these components yield abnormal wound healing. For the first time, we show a requirement for E-cadherin in single-cell wound repair, providing new mechanistic insight into this wound-healing process.

Correspondence to Susan M. Parkhurst: susanp@fhcrc.org

Abbreviations used in this paper: ChFP, mCherry fluorescent protein; GAP43, growth-associated protein 43; Lat B, latrunculin B; NC, nuclear cycle; PH-PLC, phospholipase Cγ pleckstrin homology domain; sChMCA, spaghetti squash–driven, mCherry fluorescent protein, moesin–α-helical-coiled and actin binding site; sGMCA, spaghetti squash–driven, GFP, moesin α-helical–coiled and actin binding site; shg, shotgun; sqh, spaghetti squash.

The Rockefeller University Press $30.00
J. Cell Biol. Vol. 193 No. 3 455–464
www.jcb.org/cgi/doi/10.1083/jcb.201011018

Results and discussion

Repair of single cells is mainly studied in sea urchin eggs, *Xenopus* oocytes, and cultured cells (McNeil and Steinhardt, 2003). As the first 13 nuclear divisions in the *Drosophila* embryo are not accompanied by cytokinesis, the early fly embryo can be considered as a giant single cell (Foe and Alberts, 1983). The early embryo's multinucleate nature is not unlike that of muscle cells—one of the major mammalian cell types undergoing continuous membrane tearing and using single-cell repair mechanisms (McNeil and Khakee, 1992). We used early stage *Drosophila* embryos (NC4–6) as a model to study single-cell wound repair (Fig. 1, A–C), allowing us to follow the wound repair process at the cortical surface without interference by the nuclear division process. We generated wounds on the lateral surface of these embryos by laser ablation of the cortical surface without disrupting the overlying vitelline membrane.

Analysis of single-cell wound repair in NC4 staged embryos expressing actin (sGMCA, spaghetti squash–driven, GFP, moesin α-helical–coiled and actin binding site) allowed us to divide single-cell wound repair into three distinct steps based on the repair dynamics: (1) expansion, (2) contraction, and (3) closure (Fig. 1 E). Upon wounding the cortical actin disappears and the initial wound area rapidly expands. This expansion phase occurs during the first 30–60 s after wounding (Fig. 1, D and E). Once actin accumulates in a ring flanking the wound, the diameter reduces progressively (contraction), followed by a slower closure phase (Fig. 1, D and E; Video 1). We find that neither wound size nor embryo age before cellularization affects single-cell wound repair dynamics (Fig. 1 F; Fig. S1, B and B′; Table S1; see Materials and methods).

Our assays in the early *Drosophila* embryo show that wounding triggers the rapid recruitment of actin to the edge of the hole (Fig. 1, D and D′). Actin is first detected at the wound edge 30 s after wounding. By 60 s, a continuous actin ring is observed and is maintained for at least 20 min (Fig. 1 D; Video 1). The correlation between actin recruitment and wound constriction suggests that actin may drive both the hole contraction and closure in the fly model, as has been described in the *Xenopus* oocyte single-cell repair model (Bement et al., 1999; Mandato and Bement, 2001). To test this hypothesis, we perturbed the actin cytoskeleton by treatment with latrunculin B (Lat B), an inhibitor of actin polymerization. We injected Lat B in early embryos expressing actin (sChMCA) and plasma membrane (GFP-Spider) markers. Actin was significantly disrupted (Fig. 1, G and H), resulting in altered repair dynamics with wounds expanding for more than 5 min (Fig. 1 G). Although actin is eventually recruited to the wound edge as the embryos begin to recover from the Lat B treatment, this accumulation is discontinuous, resulting in impaired contraction and a disrupted wound area that remains open 15 min after wounding compared with 5 min in control embryos (Fig. 1 G; Fig. S1 D; Video 2). In embryos with incomplete actin depolymerization (Fig. 1 H), a partial actin ring can assemble at the wound periphery, in areas where some actin still persists. Once contraction begins in one region of the leading edge, other regions with depolymerized actin are pulled along, resulting in imperfect and delayed repair (Fig. 1 H). Thus, assembly of an actin ring is required for single-cell wound repair.

Microtubules are an important component of the cell cytoskeleton, and the interaction between microtubules and actin cytoskeleton is fundamental for many cell processes (Rodriguez et al., 2003). In particular, a radial arrangement of microtubules associated with F-actin is observed at the wound border in *Xenopus* oocytes (Mandato and Bement, 2003). We evaluated the recruitment of microtubules in vivo using GFP–α-tubulin and did not detect a significant accumulation or rearrangement of microtubules at the wound edge (Fig. 1, I and I′; Fig. S1 C). However, perturbation of the microtubule network did have a negative effect on wound repair in our single-cell model. Embryos treated with colchicine (inhibitor of microtubule polymerization) show defects in actin ring assembly: some embryos fail to assemble an actin ring (n = 7/15); other embryos assemble a disorganized cable that is broad and unstable (n = 8/15; Fig. 1, J–J′′). These results indicate that although microtubules do not visibly rearrange at the wound edge, they are required for proper assembly of the actin ring.

As our analyses of cell wound repair in the early embryo show a rapid and specific recruitment of actin, we examined the contribution of myosin II in the repair response. Laser wounding of embryos coexpressing GFP-Spaghetti squash (myosin regulatory light chain, sqh-GFP) and actin (sChMCA) show that myosin II is immediately recruited to the wound edge (45 s), forms a ring that overlaps with actin throughout the repair process, and starts to dissipate 10 min after wounding (Fig. 2 A–A′′′; Video 3; Fig. S1 G). In early time points, single Z sections across the wound reveal that while the rings of actin and myosin overlap, myosin is more abundant at the leading edge of the wound, whereas actin accumulation is broader (Fig. 2 B). By 5 min the actomyosin ring split into three zones: an apical layer of actin, a middle overlapping actomyosin zone, and a basal zone enriched in myosin II (Fig. 2 B).

To further examine the role of myosin II in single-cell wound repair, we studied the effects of altering the levels of myosin genetically. Homozygous sqh^{1} mutant embryos show severe developmental defects with few embryos completing development (Wheatley et al., 1995). In embryos that do develop, the wound repair response is severely impaired: upon ablation, wounds expand normally but fail to contract (Fig. 2 C; Video 4). Kymograph analysis of these mutants shows incomplete actin ring formation at the wound edge compared with the wild type (Fig. 2 C′). Actin accumulation is significantly reduced and any cable that forms appears disorganized and unstable; as a consequence the wounds reopen (n = 4/4). Inhibition of myosin II phosphorylation by treatment with Y27632, a specific Rho kinase inhibitor (Narumiya et al., 2000), similarly disrupts cell wound repair (Fig. S1, H–H′′′; Video 4). The myosin cytoskeleton is also disrupted in Lat B–treated embryos: both actin and myosin fail to be recruited to the wound edge (not depicted). Together, our data suggest that myosin II is required for the stabilization of actin at the leading edge of wounds.

We next sought to interrogate another critical step for cell wound repair: the rapid resealing of the plasma membrane disruption. The current working model for single-cell wound repair proposes that internal vesicles directionally migrate to the wound site, then fuse with the damaged plasma membrane to

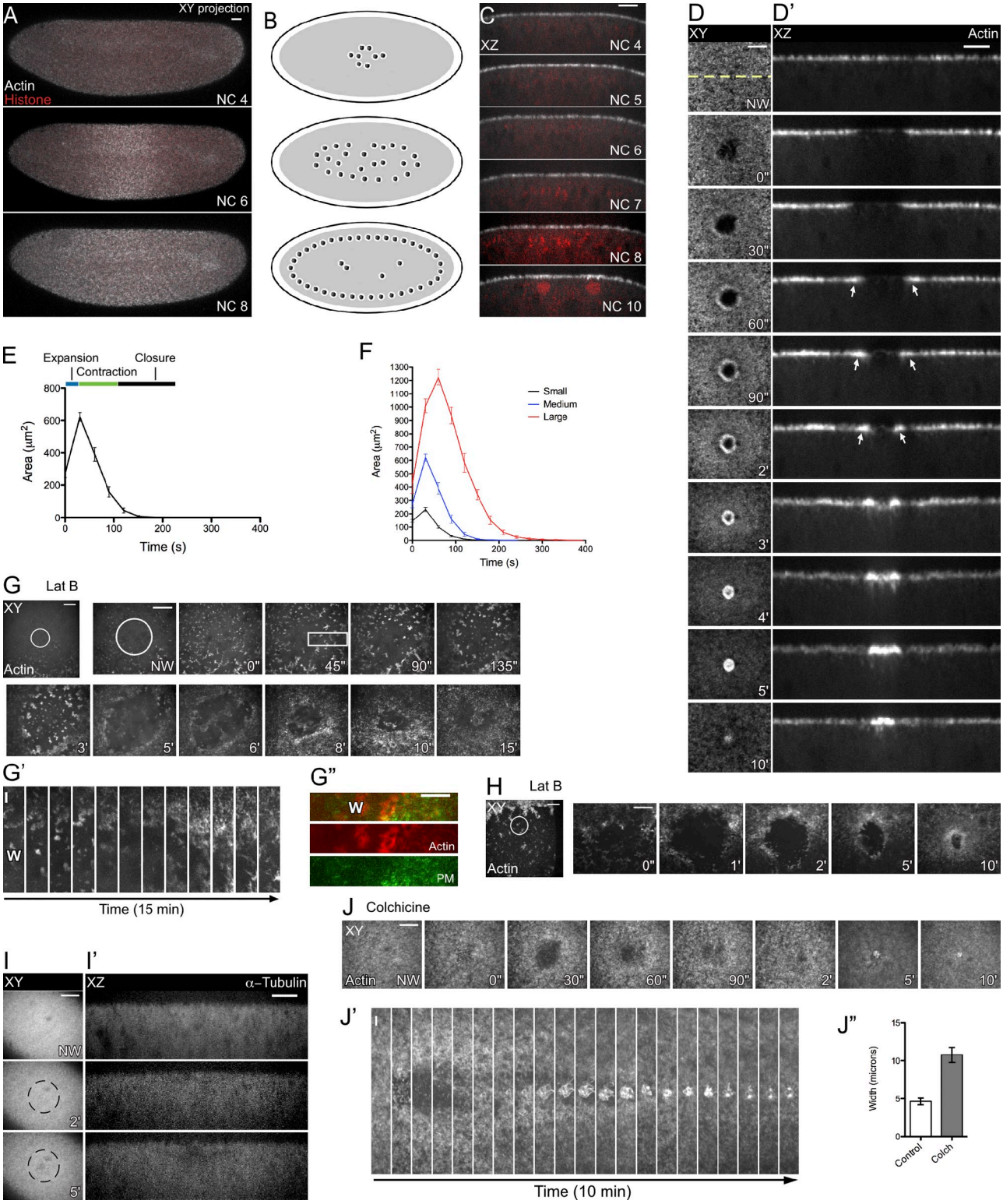

Figure 1. **The *Drosophila* embryo is a model to study single-cell wound healing.** Surface projections (A) and orthogonal sections (C) of early embryos expressing actin and histone (sGMCA; His2Av-mRFP). Nuclear cycle is indicated. (B) Cartoon depicting the embryo stages shown in A. (D and D′) Actin accumulates at the cell wound edge (arrows). Time-lapse series of surface projections (D) and cross sections (D′) of embryos expressing actin (sGMCA). Dotted line in D indicates the plane of the cross section. (E) Analysis of the phases of single cell wound repair ($n = 14$; results are given as means ± SEM). (F) Effects of wound size in cell wound repair. (small, $n = 16$; medium, $n = 14$; large, $n = 7$). (G–H) Confocal images of wound repair in embryos expressing actin and plasma membrane markers (sChMCA; GFP-Spider) and treated with Lat B ($n = 6$). Left panel shows actin depolymerization before wounding (circle indicates the ablation site). (G′) Kymograph showing failure of actin cable assembly (W, wound). (G′′) Actin and membrane recruitment are impaired. (H) In embryos exhibiting partial actin depolymerization, the actin cable is assembled in regions of the wound edge richer in actin. (I and I′) Image of a syncytial embryo expressing GFP–α-tubulin. (J and J′) Time series after wounding in embryos treated with colchicine (sGMCA). (J′) Kymograph analysis. (J′′) Ring width quantification (control = 8, colch = 8; P = 0.0003). Bars: (A, D, G, H, I, and J) 20 µm; (C, D′, G′, and I′) 10 µm; (G′′ and J′) 5 µm.

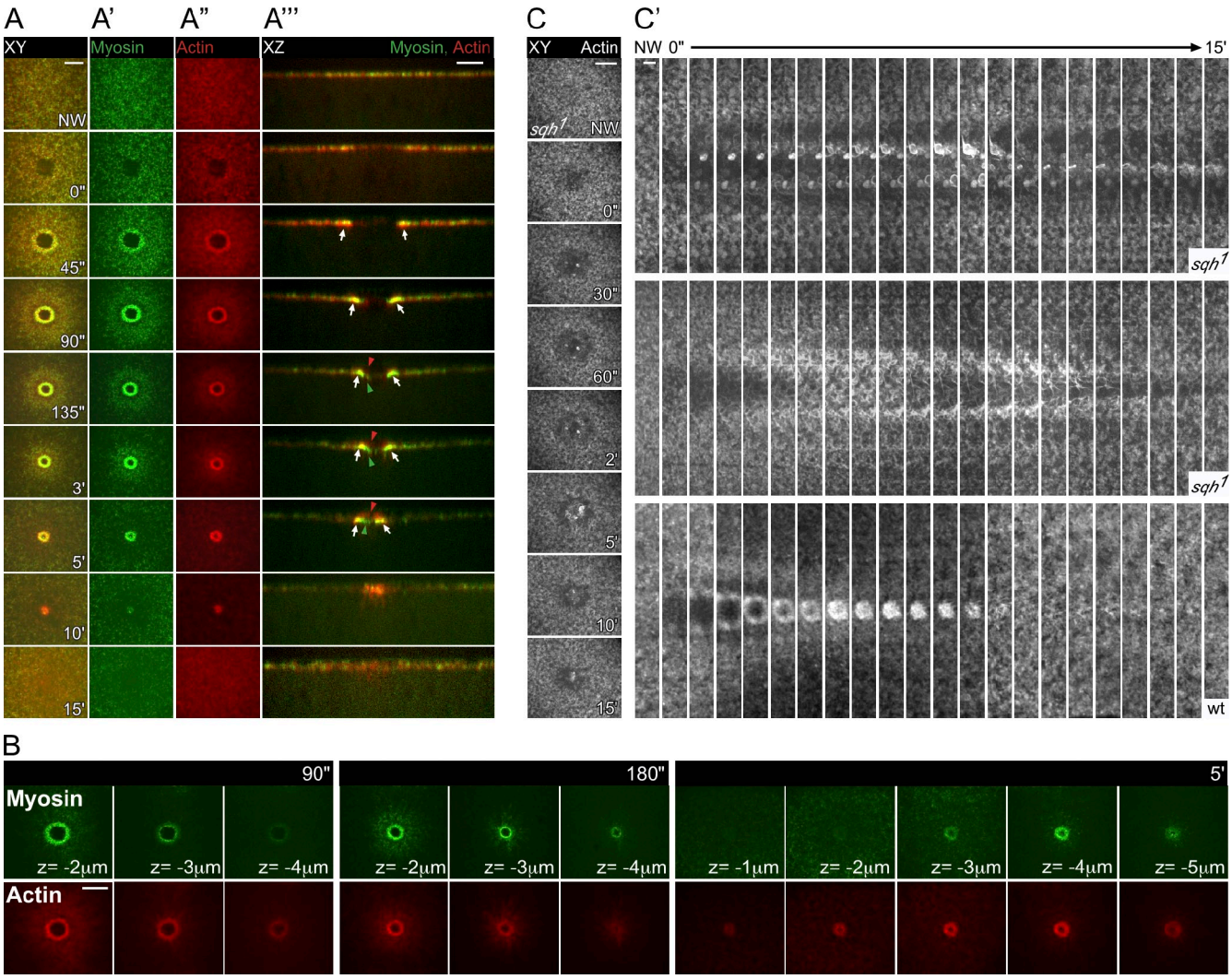

Figure 2. **Contribution of myosin II to single-cell wound repair.** (A–B) Images from early embryos expressing sChMCA; sqh-GFP. (A) Colocalization of myosin II (A′) and actin (A″). (A‴) Cross sections showing actin (red arrowhead) and myosin dynamics (green arrowheads). (B) Single Z sections of embryo in A. (C and C′) Confocal time series after the healing process in *sqh*^{1} embryos expressing actin (sGMCA; $n = 4$). (C′) Kymograph analysis, two *sqh*^{1} and a control embryo are shown. Top panel corresponds to embryo in C. Bars: (A–C) 20 µm; (A‴) 10 µm; (C′) 5 µm.

create a membrane patch (McNeil and Kirchhausen, 2005). We examined the role of plasma membrane using three membrane markers, each of which has a different mode of membrane attachment: casein kinase 1γ (GFP-Spider; Frescas et al., 2006), growth-associated protein 43 (GAP43-ChFP; Martin et al., 2010), and the pleckstrin-homology domain of PLC (GFP-PH-PLC; Pinal et al., 2006). In embryos expressing GFP-Spider along with actin (sChMCA), Spider accumulates at the leading edge of the wound internal to the actin ring (Fig. 3 A–A‴). We also observed a distinctive subcellular localization pattern of particles containing Spider expanding basally at the wound site as deep as 5 µm (Fig. 3 A‴), whereas the accumulation of actin occurs at 3 µm beneath the wound surface (Fig. 3 A″). Time lapse of GFP-Spider embryos shows accumulation at the wound edge 30 s after wounding (Fig. 3 C) and the recruitment of GFP-Spider associated with vesicles being delivered from beneath the wound and fusing with the forming membrane patch (Video 5). By 5 min after wounding a membrane plug can be observed below the wound (Fig. 3, B and B′).

The other two plasma membrane components assayed, PH-PLC and GAP43, display similar patterns to Spider. Both of these proteins localize at the wound edge shortly after wounding (1 min; Fig. 3, D–E′; Video 5) and fuse with the membrane plug beneath the wound. Significantly, the wound area is enriched in vesicles containing GAP43, which move toward and fuse with the forming membrane plug (Fig. 3 E″). Quantification of these GAP43 particles shows a higher density in the area just adjacent to the wound (Fig. 3 E‴). Our pharmacological inhibitor assays show that intact actin, myosin, and microtubule cytoskeleton are required for this plasma membrane mobilization (Fig. 1 G″; Fig. S1, F and G″). Therefore, in response to single-cell wounds, plasma membrane components are actively recruited to the wound and are responsible for forming the patch necessary to reseal the membrane hole.

As we find that membrane in the form of vesicles is rapidly recruited to the wound in a process that is actin, myosin, and microtubule dependent, important questions are how this new "plug" of membrane becomes anchored to form a continuous

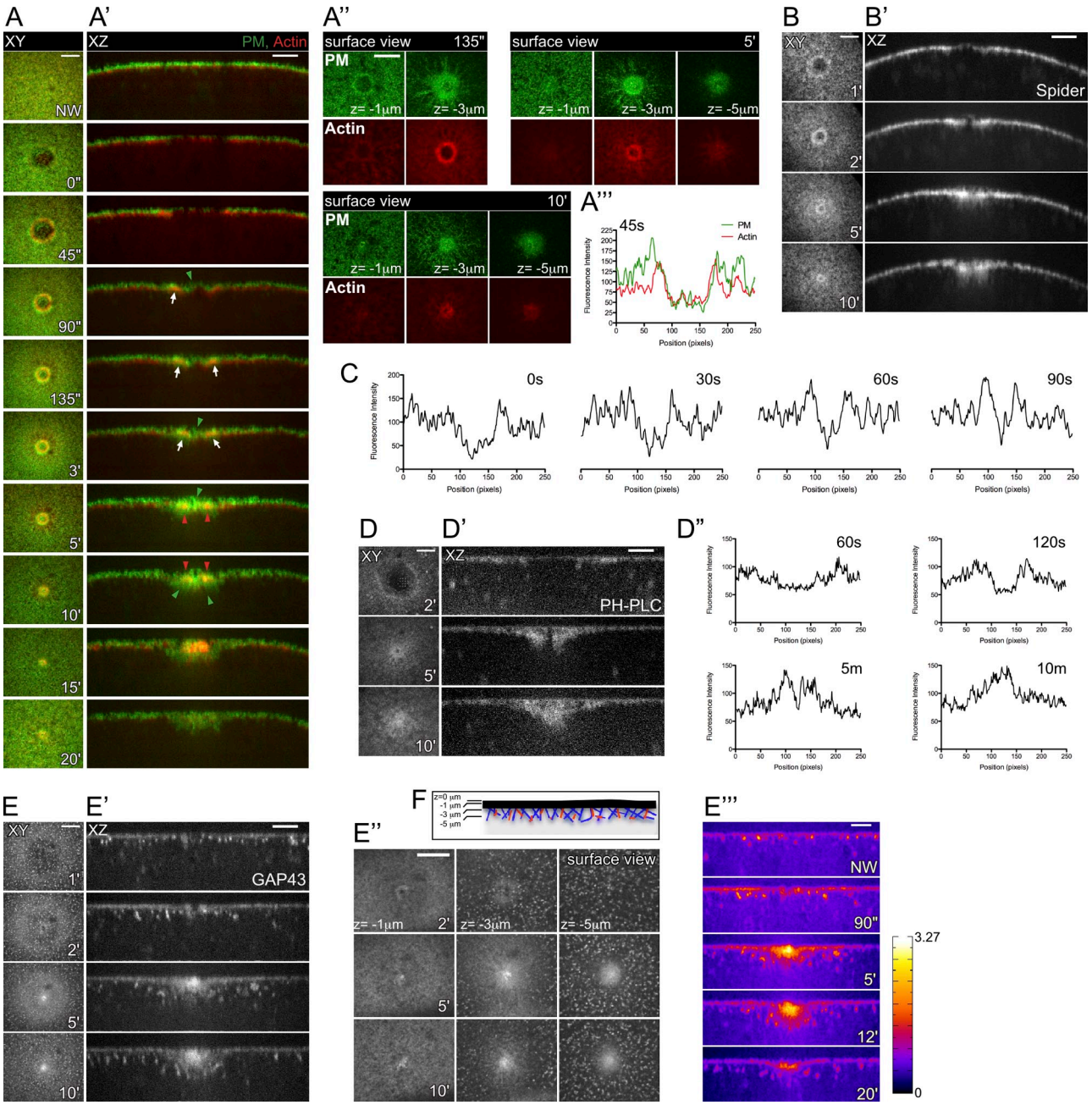

Figure 3. **Plasma membrane component involvement in single-cell wound repair.** Time series of confocal images of early embryos expressing: sChMCA; GFP-Spider (A–A′′), GFP-Spider (B and B′), PH-PLC-GFP (D and D′), and GAP43-ChFP (E–E′′). (A and A′) Actin (red arrowhead) and plasma membrane (green arrowhead) localization at the wound is indicated. (A′′) Single confocal section of specific time points from A, the position of the Z slice is indicated. Fluorescence intensity at the wound edge in SChMCA; GFP-Spider (A′′′), GFP-Spider (C), PH-PLC-GFP (D′′), and GAP43-ChFP (E′′) embryos at specific times after wounding. (F) Cartoon showing the Z planes. Plasma membrane (black line), actin (blue), and myosin (orange) are depicted. Bars: (A, A′′, B, D, E, and E′′) 20 µm; (A′, B′, D′, E′, and E′′′) 10 µm.

membrane at the cell surface and how the actin ring is associated with the plasma membrane. Studies from *Xenopus* oocytes suggest that the actin ring is anchored to the membrane at frequent intervals along the length of the wound (Mandato and Bement, 2001). This explains how actin cable contraction can mediate wound closure and how the cable can dynamically change size to adjust as closure progresses. However, it is not known how this anchoring is achieved. In epithelial wound repair, cadherin-based adherens junctions serve as anchors connecting intercellular segments of the actomyosin cable (indirectly) between neighboring cells (Wood et al., 2002). Although cadherin-based adherens junctions appear to anchor the actomyosin cable in the epithelia of stage 15 embryos, DE-cadherin has not previously been observed in the early embryo before the onset of cellularization (Tepass et al., 2001).

As cadherin expression has not been well characterized during the early stages of *Drosophila* embryo development (NC4–8), we stained early staged embryos expressing a nuclear marker (His2Av-mRFP) with a DE-cadherin–specific antibody (Oda et al., 1994). Confocal images show a punctate pattern of

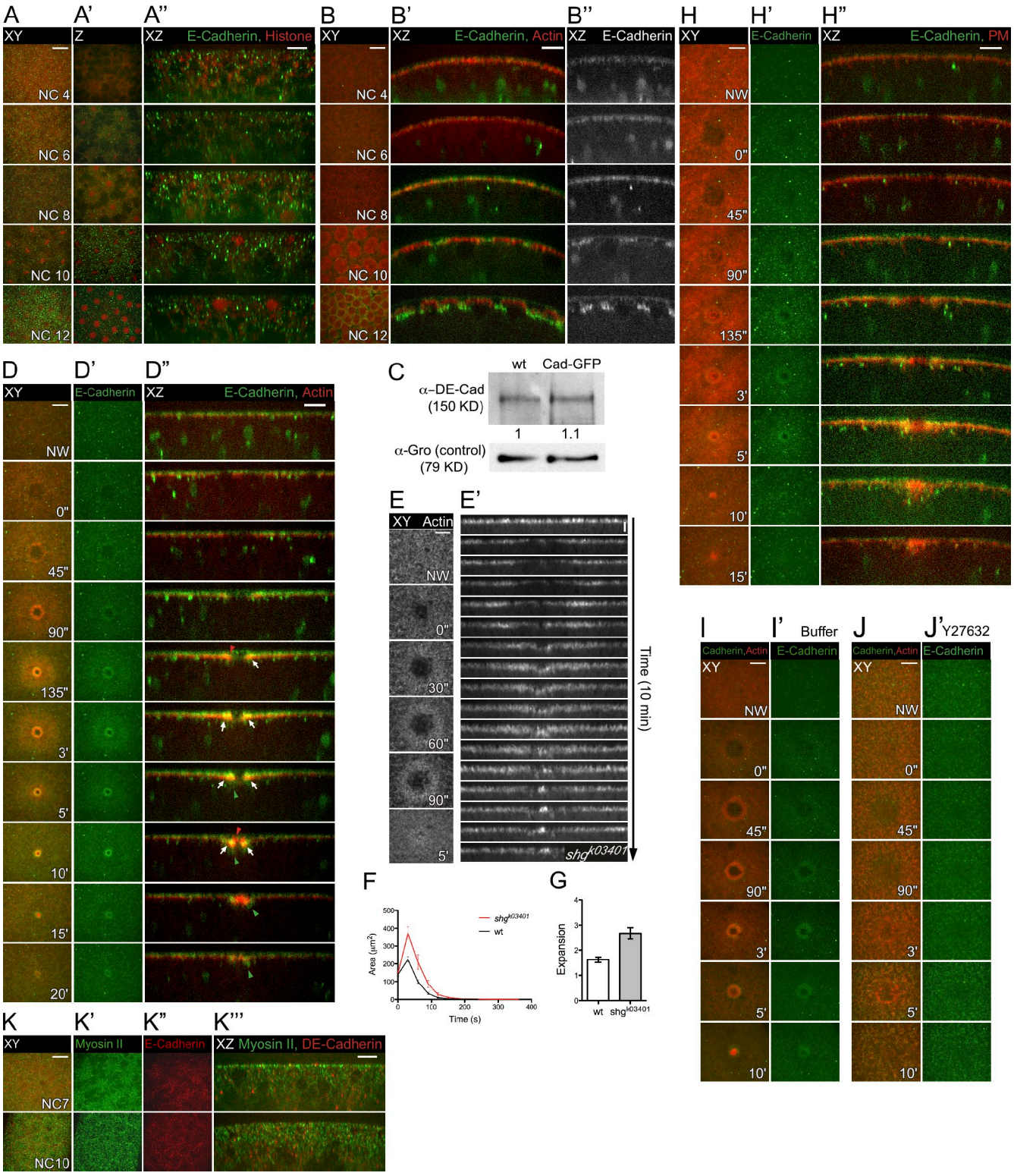

Figure 4. **DE-cadherin is required for cell wound repair.** (A–A'') DE-cadherin was detected by antibody staining in embryos expressing a nuclear marker (His2Av-mRFP). (A') Single confocal slices of the embryos in A. (B–B'') Time-lapse series of an early embryo expressing sChMCA; cadherin-GFP. (C) Western blot analysis of cadherin protein levels in embryos expressing DE-cadherin-GFP. Relative amounts of cadherin are indicated. (D–D'') Confocal images of an early embryo expressing sChMCA; cadherin-GFP. Cadherin accumulates at the wound edge and colocalizes with actin (arrows). (E–E'') Time series images of embryos maternally reduced for cadherin (sGMCA; shg^{k03401}/+; wimp/+). (E') Kymograph analysis. (F) Quantification of the wound area over time (wt, $n = 15$; shg^{k03401}, $n = 10$). (G) Quantification of wound expansion ($P = 0.0009$; all results are given as means ± SEM). (H–H'') Confocal images of an early embryo expressing cadherin-GFP and GAP43-ChFP. Actin and cadherin localization in control (I and I'; $n = 12$) and Y27632 treated embryos (J and J'; $n = 10$; sChMCA, cadherin-GFP). (L) Staining showing myosin II and DE-cadherin localization in the early embryo. Bars: (A, B, D, E, H, I, J, and K) 20 μm; (A'', B', D'', H'', and K''') 10 μm; (E') 5 μm.

cadherin expression, which can be detected as early as NC4, where it is enriched in energids but excluded from nuclei (Fig. 4, A–A′′). As the nuclei migrate toward the periphery, cadherin distributes throughout the cortical surface of the embryo (Fig. 4, A–A′′; Fig. S2, A–A′′). Live imaging of embryos expressing actin and cadherin (sChMCA; cadherin-GFP) shows cadherin at the front of the pseudocleavage furrows as early as NC12 (Fig. 4 B′; Fig. S2, B and B′). Western blot analysis of cadherin-GFP embryos corroborates that the fusion protein is not overexpressed (Fig. 4 C).

When conducting wound-healing assays in syncytial embryos expressing cadherin-GFP and actin (sChMCA), surprisingly, we observed cadherin accumulation at the edge of the repairing hole (Fig. 4, D–D′′). Cadherin localizes as a ring that overlaps with actin, and in cross sections cadherin-containing particles were observed mobilizing to the wound and accumulating at the wound border (Fig. 4 D′′; Fig. S2 C; Video 6). Cadherin at the edge of single-cell wounds could serve a similar role as in multicellular wounds, linking the actomyosin ring to the plasma membrane. By examining wounds in maternally reduced shg^{k03401} embryos, we find that cadherin is required for cell wound repair (Fig. 4, E and E′). shg^{k03401} embryos show excessive expansion (2.6-fold compared with wild type, P = 0.0009), as well as defects in actin ring assembly (Fig. 4, F and G). In the most severe cases, actin ring formation is highly irregular, suggesting a role for cadherin in anchoring the actomyosin ring to the plasma membrane in single-cell wounds. Nevertheless, these embryos eventually heal (Fig. 4 F; Video 7), suggesting a compensation mechanism perhaps by other proteins able to link the actin cytoskeleton to the plasma membrane. It will be interesting to see how other proteins involved in membrane–cytoskeleton interactions, such as ankyrin, spectrin, and ERM proteins, affect cell wound healing.

We next investigated how DE-cadherin is mobilized to the wound border. By examining wounds in embryos expressing cadherin-GFP and GAP43-ChFP, we find that membrane-associated cadherin is recruited from the area surrounding the wound where it accumulates in a ring around the membrane plug, but is excluded from the plug itself (Fig. 4, H and H′). We also detect cadherin particles trafficking toward the wound, which do not colocalize with plasma membrane vesicles (Fig. 4 H′′). To determine which cytoskeleton network mediates this cadherin recruitment to the wound edge, we first examined embryos where myosin II was disrupted (Y27632 treatment) and found that cadherin fails to accumulate at the wound edge (Fig. 4, J and J′). Actin recruitment is also impaired in Y27632-treated embryos and no significant accumulation of cadherin was observed in the resulting actin mesh (Fig. 4 J′). In contrast, embryos with a disrupted microtubule network (colchicine treatment) show normal cadherin recruitment (Fig. S3 D). Staining of early embryos with cadherin and myosin II–specific antibodies shows a similar distribution pattern during early development (Fig. 4 K–K′′′). Our data suggest that DE-cadherin is recruited from two different sources: from the membrane surrounding the wound in an actomyosin-dependent mechanism and as actomyosin-independent particles trafficking from below the wound. Recent studies have shown that myosin II mediates E-cadherin clustering in mammalian cells (Smutny et al., 2010). In single-cell wound repair myosin II could act as a scaffold or a trigger for the clustering and recruitment of cadherin to the wound leading edge.

By combining high resolution imaging and multiple fluorescence markers in both wild-type and mutant embryos, the *Drosophila* single-cell repair model facilitates the systematic analysis of specific components and provides new mechanistic insights on how these components are specifically recruited and dynamically localized during the healing process (Fig. 5). Although basic descriptions of single-cell wound repair are in place from studies in different wound models, a number of fundamental questions remain concerning the molecular details of these processes. What are the signals that recognize that the membrane has been disrupted, and how do these signals act to initiate the critical first steps of healing? In particular, what components of the actin and microtubule cytoskeletal machineries are required to drive cellular processes critical for all elements of the repair process? What are the signals that lead to disassembly of these machineries and cessation of the repair process once healing is complete? The *Drosophila* embryo provides an excellent genetic model in which to systematically define the specific series of events of single-cell wound repair and identify the molecules required for each step.

Materials and methods

Fly strains and genetics

Flies were cultured and crossed on yeast-cornmeal-molasses-malt and maintained at 25°C. The following stocks containing fluorescence fusion proteins were used: sGMCA (Kiehart et al., 2000), sChMCA (this paper), P{His2Av-mRFP1}III.1 (Bloomington Stock Center, Bloomington, IN), P{UASp-GFPS65C-alphaTub84B} (GFP–α-tubulin, Bloomington Stock Center), Spider-GFP (95–1; Morin et al., 2001), sqh^{AX3}; P{sqh-GFP}42 (sqh-GFP; Royou et al., 2004), GAP43-mCherry (membrane-mCherry; Martin et al., 2010), P{UASp-GPF-PH-PLC} (Pinal et al., 2006), and ubi-DE-cadherin-GFP (Oda and Tsukita, 2001; Kyoto Stock Center, Kyoto, Japan). Double fluorescently tagged lines were generated using standard genetic methods. Expression of UASp-GPF-PH-PLC was driven in the embryo maternally in the early embryo with P{matα4-GAL-VP16}V37 (Bloomington Stock Center).

The following mutant alleles were used: sqh^{1} (Wheatley et al., 1995), and shg^{k03401} (Bloomington Stock Center). All mutant alleles to be examined were crossed into the background of sGMCA. Reduction of maternal expression for *sqh* and *shg* was achieved as follows: for *sqh*, we generated sqh^{1} germ-line clones using the FLP-DFS system (Chou and Perrimon, 1992) with sqh^{1} FRT101/FM7 and ovo^{D1} FRT101/Y: hs-flp-F38 (Wheatley et al., 1995); for *shg*, maternally reduced shg^{k03401} embryos were generated using the *wimp* mutation (Parkhurst and Ish-Horowicz, 1991; Liu et al., 2009).

Generation of sChMCA construct and transgenics

To ubiquitously express fluorescently tagged proteins, we constructed an expression vector containing a 1.3-kb genomic fragment covering the *sqh* promoter inserted into the PstI and StuI sites of pCasper4. A fragment containing a region of the *sqh* 3′ untranslated region (530 base pairs) was then cloned downstream of the promoter into the XbaI and BamHI sites, resulting in pSqh5′+3′UTR plasmid. Primers for cloning were designed based on the sequence reported by Kiehart et al. (2000). The proteins of interest were then cloned between the *sqh* promoter and the 3′ UTR in the pSqh5′+3′UTR plasmid using the StuI and XbaI sites.

A fusion of ChFP and the moesin actin-binding site was generated as follows: the moesin actin-binding domain was amplified by PCR from genomic DNA with primers designed based on the sequence reported by Kiehart et al. (2000), then fused to ChFP and cloned in the vector previously described as a SmaI–BamHI fragment. This construct was named sChMCA for *sqh*-driven, ChFP protein, moesin α-helical-coiled and actin binding site. sChMCA construct (500 µg/ml) was injected along with the pTURBO helper

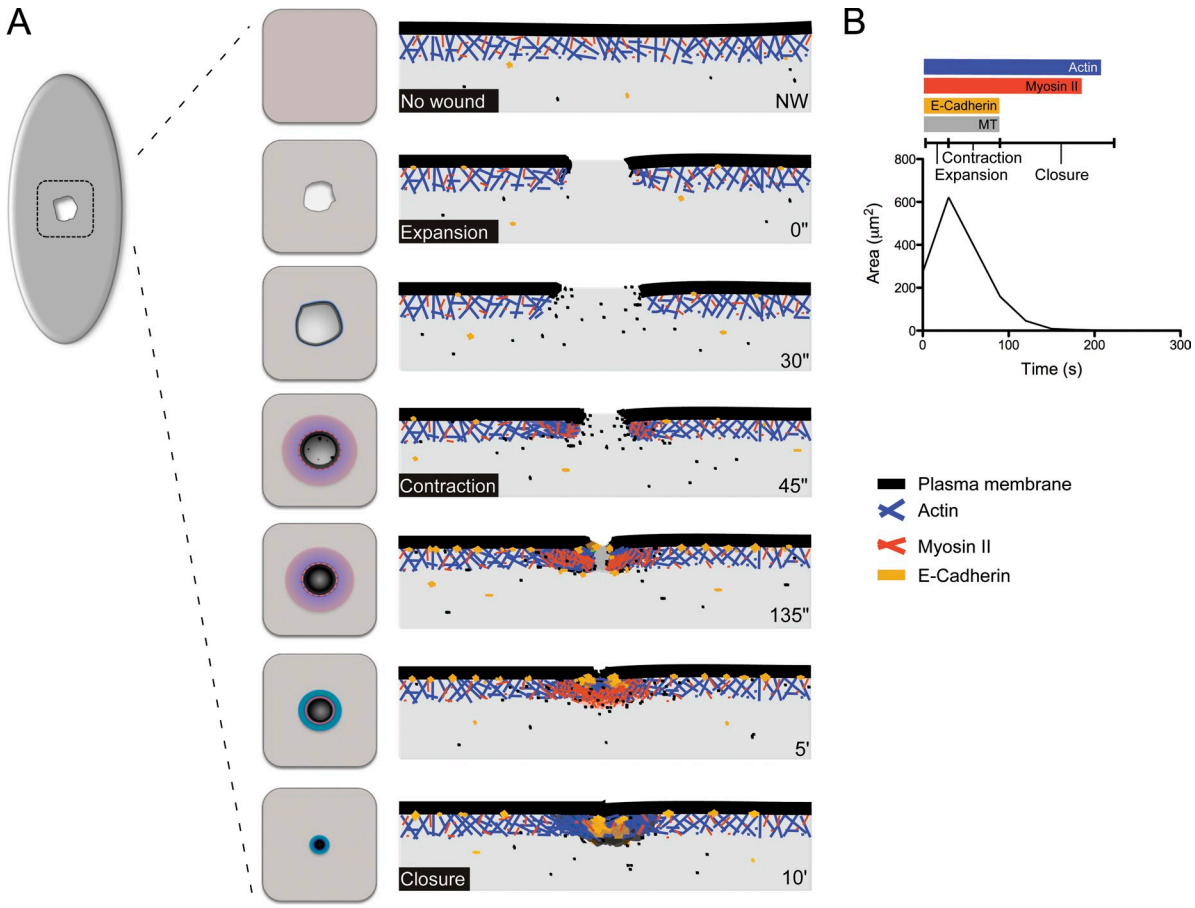

Figure 5. **Working model for single-cell wound repair in the *Drosophila* embryo.** (A) Schematic representation of the single-cell wound repair response. Surface views and cross sections are depicted. (B) Phases and components of the single-cell wound response.

plasmid (100 µg/ml) (Mullins et al., 1989) into isogenic w^{1118} flies as described previously (Spradling, 1986). Transgenics were scored by eye color and the insertions were mapped using standard genetic methods.

Embryo fixing and staining

0–1 h wild-type or His2Av-mRFP1 (to visualize nuclei) embryos were collected, dechorionated with bleach, fixed with 4% paraformaldehyde/heptane for 20 min, and devitellinized in methanol. Immunofluorescence of embryos was performed as described previously (Magie and Parkhurst, 2005). In brief, fixed embryos were incubated with the primary antibody, which has been previously preabsorbed against 0–4 h wild-type embryos. The embryos were then washed and incubated with the secondary antibody. Embryos were mounted in SlowFade Gold (Invitrogen). *Drosophila* E-cadherin was recognized using rat anti-DCad2 (1:100; Developmental Studies Hybridoma Bank, Iowa City, IA). Nonmuscle myosin was recognized using a specific antibody (1: 500; Young et al., 1991). 2° antisera used: anti–rat Alexa 488, anti–rabbit 488, or anti–rat Alexa 568 (1:1,000; Invitrogen).

Confocal fluorescent microscopy

All confocal imaging was performed at room temperature (23°C) using an LSM-510M microscope (Carl Zeiss, Inc.) with excitation at 488 nm or 543 nm, and emission collection with BP-500-550 or LP560 filters, respectively. A Plan Apochromat 20x/0.75 NA dry objective was used for imaging. Images were processed in ImageJ; all XY projections correspond to maximum projections of the entire 25-µm stack. Linear adjustments of brightness and contrast levels were applied in ImageJ. Figures were assembled in Canvas 8 (Deneva).

Embryo handling and preparation

Early embryos were collected for 0–1 h at room temperature (23°C). Embryos were hand dechorionated, dried for 5 min, and transferred to series 700 halocarbon oil (Halocarbon Products Corp.) on Greiner Lumox culture dishes made with hydrophilic gas-permeable membranes (Sigma-Aldrich). As an alternative, embryos were hand dechorionated, dried for 5 min, and transferred individually with forceps onto strips of glue dried onto no. 1.5 coverslips, and covered with halocarbon oil (Foe et al., 2000).

Drug injections

Pharmacological inhibitors were injected laterally in NC4–6 embryos mounted on a coverslip with glue and covered with series 700 halocarbon oil. The following inhibitors were used: latrunculin B (EMD) was injected at 0.5 mM; colchicine (Demecolcine; Sigma-Aldrich) was injected at 25 mM; and Rho-kinase inhibitor (Y-27632 dihydrochloride, Tocris Bioscience) was injected at 70 mM. Latrunculin B was prepared at 10 mM in DMSO (Sigma-Aldrich); colchicine and Y-27632 were prepared at 25 mM and 100 mM, respectively, in injection buffer (phosphate-buffered saline). Injected solutions are diluted 50-fold in the embryo (Foe and Alberts, 1983).

Live imaging

All imaging was performed in series 700 halocarbon oil at room temperature (23°C). Dual fluorescent live image videos were performed on a TE2000-E stand (Nikon), with 40x/1.4 NA objective lens and controlled by Volocity software (v.5.3.0; PerkinElmer). Images were acquired with 491-nm and 561-nm lasers, with a confocal spinning disc head (CSU-10; Yokogawa) equipped with a 1.5x magnifying lens, and a C9100-13 EMCCD camera (Hamamatsu Photonics). The following settings were used: exposure time 100–250 ms; laser intensity 70%; camera sensitivity 150; gain 1. The images for single-cell wound assays correspond to 27–30 µm/0.25 µm steps.

Laser wounding

Laser ablation experiments used the Micropoint Computer Controlled system (Photonic Instruments). An N_2 Micropoint laser tuned to 405 nm was focused on the cortical surface of the embryo. A region of interest

was selected and ablation was controlled by Volocity (v.5.3.0; PerkinElmer). On average, ablation time was less than 5 s, and time-lapse imaging was initiated immediately.

We established conditions to produce reproducible wound size for the single-cell wounding and tested if wound size had any effect on the repair process. By controlling the size of the selected area and the intensity of the laser, we established the conditions for three different wound sizes; the initial wound area was estimated after expansion was achieved. The wound sizes were classified as: (a) small, wound area <500 μm^2; (b) medium, with areas ranging 500–1,000 μm^2; and (c) large wounds expanding >1,000 μm^2. With the exception of the expansion phase in large wounds, no significant differences were observed between the samples (Fig. 1 F; Table S1). Unless otherwise indicated, all single-cell wound assays were conducted using small-size wounds.

Image processing, analysis, and quantification

Image series were either analyzed with Volocity software (v.5.3.0; PerkinElmer) or were exported as TIFF files then imported into ImageJ for processing. XY projections correspond to maximum projections of the entire 27–30-µm stack; in all cases XZ cross sections were taken across the middle of the wound. Linear adjustments of brightness and contrasts levels were applied in ImageJ. Measurements of wound areas and ring width were done manually with ImageJ. A Student's *t* test was used to analyze the data; $P < 0.05$ was considered to be statistically significant. All graphs include SEM bars. Quantification of fluorescence intensity was performed in ImageJ, using a region of interest (61.55 × 1.2 µm) across the middle of the wound also covering the adjacent area. Heat maps were generated with ImageJ. All measurements were downloaded into Microsoft Excel and the data were graphed using Prism 5.0c (GraphPad Software). Figures were assembled in Canvas 8 (Deneva).

Western blots

To test the levels of DE-cadherin in embryos, we performed Western blots as previously described for cadherin (Oda et al., 1994). Total embryo extracts were prepared from sChMCA; GFP–DE-cadherin or sGMCA (control) 0–1-hour-old embryos. Protein concentration was estimated using the Quantify Protein Assay System (Promega). 40 µg of proteins were mixed with SDS sample buffer and loaded on 7.5% SDS-PAGE. Immunoblots were probed with primary antibodies then secondary HRP-conjugated antibodies and processed for ECL following the manufacturer's protocol (Promega). DE-cadherin–specific DCad2 monoclonal antibody was used (1:50; Developmental Studies Hybridoma Bank); as loading control we used a monoclonal antibody against Groucho (1:300; Developmental Studies Hybridoma Bank). Secondary antibodies used were anti–rat HRP and anti–mouse HRP (1:15,000; Jackson ImmunoResearch Laboratories, Inc.).

Online supplemental material

Fig. S1 shows single-cell wound healing of NC6 and NC10 embryos expressing actin and nuclei markers, the microtubule response to wounding, controls for the pharmacological perturbation assays, and wound healing in Y27632-treated embryos. Fig. S2 includes the characterization of DE-cadherin expression in the early embryo and the effect of microtubule disruption in cadherin recruitment. Table S1 shows the parameters of the single-cell wound response. Video 1 shows actin recruitment in response to cell wounding. Video 2 shows the effects of disrupting the actin or microtubule cytoskeleton in single-cell wound repair. Video 3 shows myosin II accumulation at single-cell wounds. Video 4 shows the effects of myosin disruption on the wound repair process. Video 5 shows the recruitment of plasma membrane components to single-cell wounds. Video 6 shows recruitment of DE-cadherin to single-cell wounds. Video 7 shows the wound response in *shgk*^{03401} embryos. Online supplemental material is available at http://www.jcb.org/cgi/content/full/jcb.201011018/DC1.

We thank J. Molk, H. Rincón, V. Vasioukhin, and Parkhurst laboratory members for their interest, advice, and comments on the manuscript; and J. Priess and J. Molk for microscope use and imaging advice. We thank R.E. Karess, D.P. Kiehart, J. Lippincott-Schwartz, A.C. Martin, H. Oda, F. Payré, F. Pichaud, E.F. Wieschaus, the Bloomington/Kyoto Stock Centers, and the Developmental Studies Hybridoma Bank for antibodies, flies and other reagents used in this study.

This work was supported by National Institutes of Health grant GM092731 to S.M. Parkhurst.

Submitted: 3 November 2010
Accepted: 1 April 2011

References

Bement, W.M., C.A. Mandato, and M.N. Kirsch. 1999. Wound-induced assembly and closure of an actomyosin purse string in *Xenopus* oocytes. *Curr. Biol.* 9:579–587. doi:10.1016/S0960-9822(99)80261-9

Bement, W.M., H.Y. Yu, B.M. Burkel, E.M. Vaughan, and A.G. Clark. 2007. Rehabilitation and the single cell. *Curr. Opin. Cell Biol.* 19:95–100. doi:10.1016/j.ceb.2006.12.001

Chou, T.B., and N. Perrimon. 1992. Use of a yeast site-specific recombinase to produce female germline chimeras in *Drosophila*. *Genetics*. 131:643–653.

Coulombe, P.A., M.E. Hutton, R. Vassar, and E. Fuchs. 1991. A function for keratins and a common thread among different types of epidermolysis bullosa simplex diseases. *J. Cell Biol.* 115:1661–1674. doi:10.1083/jcb.115.6.1661

Fein, A., and M. Terasaki. 2005. Rapid increase in plasma membrane chloride permeability during wound resealing in starfish oocytes. *J. Gen. Physiol.* 126:151–159. doi:10.1085/jgp.200509294

Foe, V.E., and B.M. Alberts. 1983. Studies of nuclear and cytoplasmic behaviour during the five mitotic cycles that precede gastrulation in *Drosophila* embryogenesis. *J. Cell Sci.* 61:31–70.

Foe, V.E., C.M. Field, and G.M. Odell. 2000. Microtubules and mitotic cycle phase modulate spatiotemporal distributions of F-actin and myosin II in *Drosophila* syncytial blastoderm embryos. *Development*. 127:1767–1787.

Frescas, D., M. Mavrakis, H. Lorenz, R. Delotto, and J. Lippincott-Schwartz. 2006. The secretory membrane system in the *Drosophila* syncytial blastoderm embryo exists as functionally compartmentalized units around individual nuclei. *J. Cell Biol.* 173:219–230. doi:10.1083/jcb.200601156

Galko, M.J., and M.A. Krasnow. 2004. Cellular and genetic analysis of wound healing in *Drosophila* larvae. *PLoS Biol.* 2:E239. doi:10.1371/journal.pbio.0020239

Gilbert, R.J. 2002. Pore-forming toxins. *Cell. Mol. Life Sci.* 59:832–844. doi:10.1007/s00018-002-8471-1

Kiehart, D.P., C.G. Galbraith, K.A. Edwards, W.L. Rickoll, and R.A. Montague. 2000. Multiple forces contribute to cell sheet morphogenesis for dorsal closure in *Drosophila*. *J. Cell Biol.* 149:471–490. doi:10.1083/jcb.149.2.471

Liu, R., M.T. Abreu-Blanco, K.C. Barry, E.V. Linardopoulou, G.E. Osborn, and S.M. Parkhurst. 2009. Wash functions downstream of Rho and links linear and branched actin nucleation factors. *Development*. 136:2849–2860. doi:10.1242/dev.035246

Magie, C.R., and S.M. Parkhurst. 2005. Rho1 regulates signaling events required for proper *Drosophila* embryonic development. *Dev. Biol.* 278:144–154. doi:10.1016/j.ydbio.2004.10.022

Mandato, C.A., and W.M. Bement. 2001. Contraction and polymerization cooperate to assemble and close actomyosin rings around *Xenopus* oocyte wounds. *J. Cell Biol.* 154:785–797. doi:10.1083/jcb.200103105

Mandato, C.A., and W.M. Bement. 2003. Actomyosin transports microtubules and microtubules control actomyosin recruitment during *Xenopus* oocyte wound healing. *Curr. Biol.* 13:1096–1105. doi:10.1016/S0960-9822(03)00420-2

Martin, P., and S.M. Parkhurst. 2004. Parallels between tissue repair and embryo morphogenesis. *Development*. 131:3021–3034. doi:10.1242/dev.01253

Martin, A.C., M. Gelbart, R. Fernandez-Gonzalez, M. Kaschube, and E.F. Wieschaus. 2010. Integration of contractile forces during tissue invagination. *J. Cell Biol.* 188:735–749. doi:10.1083/jcb.200910099

McNeil, P.L., and R. Khakee. 1992. Disruptions of muscle fiber plasma membranes. Role in exercise-induced damage. *Am. J. Pathol.* 140:1097–1109.

McNeil, P.L., and T. Kirchhausen. 2005. An emergency response team for membrane repair. *Nat. Rev. Mol. Cell Biol.* 6:499–505. doi:10.1038/nrm1665

McNeil, P.L., and R.A. Steinhardt. 2003. Plasma membrane disruption: repair, prevention, adaptation. *Annu. Rev. Cell Dev. Biol.* 19:697–731. doi:10.1146/annurev.cellbio.19.111301.140101

Morin, X., R. Daneman, M. Zavortink, and W. Chia. 2001. A protein trap strategy to detect GFP-tagged proteins expressed from their endogenous loci in *Drosophila*. *Proc. Natl. Acad. Sci. USA*. 98:15050–15055. doi:10.1073/pnas.261408198

Mullins, M.C., D.C. Rio, and G.M. Rubin. 1989. cis-acting DNA sequence requirements for P-element transposition. *Genes Dev.* 3:729–738. doi:10.1101/gad.3.5.729

Narumiya, S., T. Ishizaki, and M. Uehata. 2000. Use and properties of ROCK-specific inhibitor Y-27632. *Methods Enzymol.* 325:273–284. doi:10.1016/S0076-6879(00)25449-9

Oda, H., and S. Tsukita. 2001. Real-time imaging of cell-cell adherens junctions reveals that *Drosophila* mesoderm invagination begins with two phases of apical constriction of cells. *J. Cell Sci.* 114:493–501.

Oda, H., T. Uemura, Y. Harada, Y. Iwai, and M. Takeichi. 1994. A *Drosophila* homolog of cadherin associated with armadillo and essential for embryonic cell-cell adhesion. *Dev. Biol.* 165:716–726. doi:10.1006/dbio.1994.1287

Parkhurst, S.M., and D. Ish-Horowicz. 1991. wimp, a dominant maternal-effect mutation, reduces transcription of a specific subset of segmentation genes in *Drosophila*. *Genes Dev.* 5:341–357. doi:10.1101/gad.5.3.341

Petrof, B.J., J.B. Shrager, H.H. Stedman, A.M. Kelly, and H.L. Sweeney. 1993. Dystrophin protects the sarcolemma from stresses developed during muscle contraction. *Proc. Natl. Acad. Sci. USA*. 90:3710–3714. doi:10.1073/pnas.90.8.3710

Pinal, N., D.C. Goberdhan, L. Collinson, Y. Fujita, I.M. Cox, C. Wilson, and F. Pichaud. 2006. Regulated and polarized PtdIns(3,4,5)P3 accumulation is essential for apical membrane morphogenesis in photoreceptor epithelial cells. *Curr. Biol.* 16:140–149. doi:10.1016/j.cub.2005.11.068

Rodriguez, O.C., A.W. Schaefer, C.A. Mandato, P. Forscher, W.M. Bement, and C.M. Waterman-Storer. 2003. Conserved microtubule-actin interactions in cell movement and morphogenesis. *Nat. Cell Biol.* 5:599–609. doi:10.1038/ncb0703-599

Royou, A., C. Field, J.C. Sisson, W. Sullivan, and R. Karess. 2004. Reassessing the role and dynamics of nonmuscle myosin II during furrow formation in early *Drosophila* embryos. *Mol. Biol. Cell*. 15:838–850. doi:10.1091/mbc.E03-06-0440

Smutny, M., H.L. Cox, J.M. Leerberg, E.M. Kovacs, M.A. Conti, C. Ferguson, N.A. Hamilton, R.G. Parton, R.S. Adelstein, and A.S. Yap. 2010. Myosin II isoforms identify distinct functional modules that support integrity of the epithelial zonula adherens. *Nat. Cell Biol.* 12:696–702. doi:10.1038/ncb2072

Spradling, A.C. 1986. P element-mediated transformation. *In Drosophila*: A practical approach. D.B. Roberts, editor. IRL Press, Oxford. 175–197.

Stramer, B., W. Wood, M.J. Galko, M.J. Redd, A. Jacinto, S.M. Parkhurst, and P. Martin. 2005. Live imaging of wound inflammation in *Drosophila* embryos reveals key roles for small GTPases during in vivo cell migration. *J. Cell Biol.* 168:567–573. doi:10.1083/jcb.200405120

Tepass, U., G. Tanentzapf, R. Ward, and R. Fehon. 2001. Epithelial cell polarity and cell junctions in *Drosophila*. *Annu. Rev. Genet.* 35:747–784. doi:10.1146/annurev.genet.35.102401.091415

Wheatley, S., S. Kulkarni, and R. Karess. 1995. *Drosophila* nonmuscle myosin II is required for rapid cytoplasmic transport during oogenesis and for axial nuclear migration in early embryos. *Development*. 121:1937–1946.

Wood, W., A. Jacinto, R. Grose, S. Woolner, J. Gale, C. Wilson, and P. Martin. 2002. Wound healing recapitulates morphogenesis in *Drosophila* embryos. *Nat. Cell Biol.* 4:907–912. doi:10.1038/ncb875

Young, P.E., T.C. Pesacreta, and D.P. Kiehart. 1991. Dynamic changes in the distribution of cytoplasmic myosin during *Drosophila* embryogenesis. *Development*. 111:1–14.